# Quantitative RyR1 reduction and loss of calcium sensitivity of RyR1Q1970fsX16+A4329D cause cores and loss of muscle strength

Moran Elbaz[1], Alexis Ruiz[1], Christoph Bachmann[1], Jan Eckhardt[1], Pawel Pelczar[2], Elisa Venturi[3], Chris Lindsay[3,4], Abigail D. Wilson[3], Ahmed Alhussni[3], Thomas Humberstone[3], Laura Pietrangelo[5], Simona Boncompagni[5], Rebecca Sitsapesan[3], SusanTreves[1,6], Francesco Zorzato[1,6,*]

[1]Departments of Anaesthesia and Biomedicine, Basel University Hospital, Hebelstrasse 20, 4031 Basel, Switzerland

[2]Center for Transgenic Models, University of Basel, Mattenstrasse 22, 4002 Basel, Switzerland

[3]Department of Pharmacology, University of Oxford, Mansfield Road, Oxford OX1 3QT, U.K.

[4]Department of Chemistry, Chemistry Research Laboratory, University of Oxford, Oxford, U.K.

[5]Center for Research on Ageing and Translational Medicine & DNICS - Dept. of Neuroscience, Imaging and Clinical Sciences, Univ. G. d'Annunzio, 66100 Chieti, Italy

[6]Department of Life Science and Biotechnology, University of Ferrara, Via Borsari 46, 44100, Ferrara, Italy

[*]To whom correspondence should be sent: Prof Francesco Zorzato, LAB 408 ZLF, Hebelstrasse 20, 4031 Basel, Switzerland. E-mail: fzorzato@usb.ch, zor@unife.it Tel. +41612652371; FAX +41612653704

**Abstract**

Recessive *RYR1* mutations cause congenital myopathies including multiminicore disease, congenital fiber type disproportion and centronuclear myopathy. We created a mouse model knocked-in for the Q1970fsX16+A4329D *RYR1* mutations, which are isogenic with those identified in a severely affected child with multiminicore disease. During the first 20 weeks after birth the body weight and the spontaneous running distance of the mutant mice were 20% and 50% lower compared to WT littermates. Skeletal muscles from mutant mice contained "cores" characterized by severe myofibrillar disorganization associated with misplacement of mitochondria. Furthermore, their muscles developed less force, and had smaller electrically evoked calcium transients. Mutant RyR1 channels incorporated into lipid bilayers were less sensitive to calcium and caffeine, but no change in single-channel conductance was observed**.** Our results demonstrate that the phenotype of the RyR1Q1970fsX16+A4329D heterozygous mice recapitulates the clinical picture of multiminicore patients, and provide evidence of the molecular mechanisms responsible for skeletal muscle defects.

# Introduction

The propagation of the action potential deep into the muscle fiber by means of the transverse tubular system (i.e. transverse tubules, TTs) leads to a massive release of $Ca^{2+}$ from the sarcoplasmic reticulum (SR) throughout the entire length of the muscle fiber via a process called excitation-contraction coupling (ECC) (1-3). The voltage dependent release of $Ca^{2+}$ from the SR initiates muscle contraction, while muscle relaxation is brought about by SR $Ca^{2+}$ uptake via the sarco(endo)plasmic reticulum CaATPAse (SERCA) (4). ECC occurs at the contact region between the TT and the SR membrane, a domain encompassing a macromolecular complex made up by the dihydropyridine receptor (DHPR), the ryanodine receptor (RyR1), calsequestrin as well as other accessory proteins (5-7). Under resting conditions the DHPR inhibits the RyR1 but upon TT membrane depolarization, DHPRs generate an orthograde signal to the RyR1s causing opening of the $Ca^{2+}$ channel; in turn, RyR1s send a retrograde signal to DHPRs which are important to support DHPR channel activity (8-10).

Because of their central role in ECC, alterations of RyR1 function are the primary cause of a number of neuromuscular disorders including malignant hyperthermia susceptibility (MH; MIM #145600), central core disease (CCD; MIM #11700), specific forms of multi-minicore disease (MmD; MIM # 255320) and centronuclear myopathy (CNM; MIM # 255320) (for a recent reviews see (11)), as well as critical care illnesses such as sepsis and intensive care polyneuropathy (12,13).

Experimental results obtained from many laboratories indicate that *RYR1* mutations result mainly in four types of channel defects (14): The first class of *RYR1* mutations (MH) causes the channels to become hypersensitive to activation by electrical and pharmacological stimuli. The second class of *RYR1* mutations (CCD) results in leaky channels leading to depletion of $Ca^{2+}$ from intracellular (SR) stores. The third class of *RYR1* mutations linked to some forms of CCD causes excitation–contraction uncoupling, whereby activation of the

voltage sensing DHPR is unable to cause release of $Ca^{2+}$ from the SR. The fourth class is characterized by a decrease of mutant RyR1 channels expression on SR membranes and is distinctive of recessive *RYR1* mutations (15-17). Most studies on ryanodinopathies have so far focused on the pathophysiology of RyR1 mutations belonging to class 1, 2 and 3 and few studies have focused on the pathophysiological changes induced by recessive (class 4) *RYR1* mutations (18-20).

Patients with congenital myopathies linked to recessive (class 4) *RYR1* mutations typically exhibit proximal muscle weakness that can be accounted for at least in part, by the reduction of RyR1 content observed in muscle biopsies (11,15-17). This decrease of RyR1 is also accompanied by a moderate fiber atrophy, which may additionally contribute to the decrease of muscle strength. Furthermore, in adult muscle fibers from patients carrying recessive *RYR1* mutations an epigenetic loop leading to (i) increased content of HDAC-4 and HDAC-5; (ii) increased genomic *RYR1* gene methylation; (iii) reduction of the transcription of MEF-2 dependent genes; (iv) depletion of muscle specific miR-1 and -133, as well as miR-22 and -124 (20) is also activated which may further impinge on muscle function.

A number of unsolved questions have been raised concerning the pathophysiological mechanisms and abnormal signaling pathways that are activated in the muscles of patients carrying recessive *RYR1* mutations. In particular, what mechanisms are responsible for the reduction of RyR1 expression? What is the role of epigenetic changes in the pathomechanism of disease? To address these questions, we have developed a mouse model carrying recessive *RYR1* compound heterozygous mutations isogenic with *RYR1* mutations identified in severely affected MmD patients (16,21), namely the *RYR1* p.Q1970fsX16 (in exon 36) plus p.4329D (in exon 91). Comparison of compound heterozygous RyR1Q1970fsX16+A4329D mice with age-matched wild-type littermates showed that the phenotype of the mutant mice recapitulates that of MmD patients. On the basis of these results we believe that the compound heterozygous *RYR1* mutant mouse is a good model for congenital myopathies linked to

recessive *RYR1* mutations; this double knock-in mouse which can be exploited for preclinical studies aimed at developing therapeutic strategies to treat neuromuscular disorders linked to recessive *RYR1* mutations.

## Results

### *In vivo* phenotype of RyR1Q1970fsX16+A4329D compound heterozygous mice

The presence of the frame shift mutation in ex36 and missense mutation in ex91 of the *RYR1* gene in the mice that were used for the experiments was confirmed by diagnostic digestion of PCR fragments with the restriction enzyme *PvuII* (Supplementary Figure 1). Compound RyR1Q1970fsX16+A4329D mice did not exhibit a postnatal lethal phenotype or defects in embryonic development and were undistinguishable from WT or heterozygous *RYR1* mutant carrier littermates (Fig. 1a). However, their post-natal development was remarkably different compared to WT or heterozygous *RYR1* mutant carrier littermates. Analysis of the growth curves performed during the observation period of 18 weeks indicates that both male and female RyR1Q1970fsX16+A4329D double knock-in mice exhibit a 20% lower body weight compared to that of WT littermates (Fig. 1b and 1c). The growth curves of mice carrying the single *RYR1* heterozygous mutation were similar to those of their WT littermates (Supplementary Figure 3). The reduced growth rate occurred after weaning since at E17-E18 and up to two weeks of post-natal developments, the mice of the four different genotypes, namely WT, RyR1Q1970fsX16, RyR1A4329D and RyR1Q1970fsX16+A4329D had a similar body weight.

### RyR1Q1970fsX16+A4329D compound heterozygous mutations affect voluntary motor activity.

We next investigated the skeletal muscle phenotype *in vivo* by analyzing the running capacity of the mice, using the voluntary running wheel set-up. Such an experimental system avoids potential problems linked to the effect of the circadian rhythm on animal activity since the mice have free access to the running wheel. We measured the dark phase (5 pm to 5 am) running distance of three-months-old RyR1Q1970fsX16+A4329D mice and compared it to

that of WT littermates (Fig. 2). Two weeks of training improved running performance in both mouse groups; nevertheless, on day 21 the total dark phase running distance of WT mice was approx. 68% greater compared to that of RyR1Q1970fsX16+A4329D mice (Fig. 2a)(167.52±5.43 km n=9 vs 99.34±9.98 km n=7 for WT and p.Q1970fsX16+p.A4329D, respectively; mean±s.e.m., Mann-Whitney two-tailed test, calculated over the 21 days of running $p<0.05$). The shorter running distance was also associated with a lower median cruise speed of the RyR1Q1970fsX16+A4329D mice compared to that of WT littermates (Fig. 2b)(Mann-Whitney two-tailed test, calculated over 21 day running period $p<0.05$).

## Decrease of isometric force development in RyR1Q1970fsX16+A4329D heterozygous mice

The reduced speed and total running distance of the RyR1Q1970fsX16+A4329D heterozygous mice may result from alterations of the mechanical properties of skeletal muscles and/or metabolic effects. To discriminate between these two possibilities, we investigated the mechanical properties of intact EDL and soleus muscles from wild-type and RyR1Q1970fsX16+A4329D mice upon delivery of a single action potential (Fig. 3a and 3b) or by a train of pulses of 1.0 msec duration delivered at 150 Hz for 400 msec (EDL) or 120 Hz for 1100 msec (soleus) to obtain maximal tetanic contracture (Fig. 3c and 3d). The averaged specific twitch peak force induced by a single action potential in EDL from RyR1Q1970fsX16+A4329D mice was approximately 60% lower compared to that obtained from EDLs from WT mice (88.39±21.80 mN/mm$^2$ , n=10 vs 35.76±9.87$^*$ mN/mm$^2$, n=10, respectively; mean± S.D.; Mann-Whitney two-tailed test $^*p<0.01$; Supplementary Table 3). Soleus muscles from RyR1Q1970fsX16+A4329D mice also exhibited a decrease of specific twitch peak force compared to soleus muscles from WT littermates (55.65±23.33 mN/mm$^2$, n=9 vs 28.46±5.21$^*$ mN/mm$^2$, n=10, respectively; mean± S.D.; Mann-Whitney two-tailed test $^*$ $p<0.01$; Supplementary Table 3). The decrease of twitch force in soleus was less pronounced

compared to that occurring in EDL muscles (approx. 50% vs 60% for soleus and EDL, respectively). The decrease of specific twitch force was paralleled by differences of the twitch kinetics (Supplementary Table 3). In particular, the time to peak both in EDL and soleus muscles from RyR1Q1970fsX16+A4329D mice were faster (10.65±1.77* msec n=10 and 24.23±1.74* msec, n=10, respectively) compared to those of WT littermates (14.70±1.96 msec, n= 10 and 28.44±3.19 msec, n=10, respectively; mean±S.D., Mann-Whitney two-tailed test *$p<0.01$). Additionally, soleus muscles from RyR1Q1970fsX16+A4329D mice showed a faster half relaxation time compared to those of WT littermates (34.38±4.00 msec, n=10 and 40.89±6.92 msec, n=9, respectively; mean±S.D., Mann-Whitney two-tailed test *$p<0.01$). Furthermore, the presence of the compound heterozygous *RYR1* mutations affected the force developed during tetanic contractures. The maximal specific tetanic force developed in EDL muscles from RyR1Q1970fsX16+A4329D mice during stimulation with a train of pulses delivered at 150 Hz was approximately 30% lower than that developed in EDL muscles from WT mice (296±58.6* $mN/mm^2$, n=10 vs 415.±79.76 $mN/mm^2$, n=10, respectively; mean±S.D., *$p<0.05$) (Fig.3c and 3e). A similar decrease in maximal specific tetanic force generation was also observed in soleus muscles from RyR1Q1970fsX16+A4329D mice (Fig. 3d and 3f) (151±23.26* $mN/mm^2$, n=9) compared to WT (218.58±48.4 $mN/mm^2$ , n=9, mean±S.D., Mann-Whitney two-tailed test * $p<0.05$). The decrease in force output is not due to fast-to-slow fiber transition since we didn't observed any changes in the expression of myosin heavy chain (MyHC) isoforms in EDL and soleus muscles (Fig. 4). The reduced peak tetanic force observed in EDL and soleus muscles from the RyR1Q1970fsX16+A4329D mice is consistent with a decrease of approx. 10% of the wet weight of both EDL (10.10±1.51* mg, n=10) and soleus (10.95±1.12* mg, n=10) muscles, compared to that of muscles from WT mice (12.77±0.99 mg and 12.24±1.02 mg, n=10 and n=9, respectively; mean± S.D.; Mann-Whitney two-tailed test *$p<0.05$)(Supplementary Table 3). EDL muscles from RyR1Q1970fsX16+A4329D mice also showed a shift of minimal Feret's fiber diameter

distribution to lower values, indicating an atrophy of the fast fibers a result that is consistent with the impaired muscle performance observed by *in vivo* and *in vitro*. Soleus muscles from RyR1Q1970fsX16+A4329D mice were not different from those isolated from WT mice (Fig. 4) a result which likely reflects differences in fiber type composition between EDL and soleus muscles. The latter muscles are composed of: 60% slow type I fibers and by approximately 40 % fast oxidative type 2A/X fibers while EDL contain approximately 90% fiber type 2B/2X and small fraction of type I fibers (22, 23).

## RyR1 content is decreased in muscles from RyR1Q1970fsX16+A4329D mice.

The decreased muscle strength observed in RyR1Q1970fsX16+A4329D mice is a feature also shared by the heterozygous RyR1Q1970fsX16 mice (24). The latter mouse model, as well as the human patient isogenic for these mutations, also shows a decrease of the RyR1 protein content in total muscle homogenates (16), and this observation may further explain the poor muscle performance of this mouse model. Thus, we investigated the expression levels of the major protein components (and/or their transcripts) encompassing the supramolecular complex involved in ECC coupling in total homogenates of EDL and soleus muscles from WT and RyR1Q1970fsX16+A4329D mice (Fig.5a). The total content of calsequestrin 1, SERCA1, SERCA2 and ß1a was similar in total homogenates from EDL and soleus muscles of WT and RyR1Q1970fsX16+A4329D mice. However, compared to WT, the RyR1 content in total homogenates of EDL and soleus muscles from RyR1Q1970fsX16+A4329D mice was reduced by 68.0±20.0% and 64.0±22.0% (mean±S.D., n=11; Mann-Whitney two-tailed test $p<0.0001$), respectively. qPCR analysis confirmed that the RYR1 transcript was significantly reduced (Mann-Whitney two-tailed test $p<0.0005$) in RyR1Q1970fsX16+A4329D mice compared to WT littermates (n=8 and n=9, respectively), whereas CACNA1S (n=9) and RYR3 transcript levels were unchanged (n=7 and n=9, in

RyR1Q1970fsX16+A4329D and WT, respectively)(Fig. 5b). Since skeletal muscles from human patients show significant up-regulation of transcripts encoding enzymes involved in epigenetic regulation, including histone deacetylases (HDACs) and DNA methyltransferases (DNMT) (20), we investigated these as well. Significant up-regulation of HDAC-4 protein was observed in both EDL and soleus muscles from RyR1Q1970fsX16+A4329D mice (Mann-Whitney two-tailed test $^{*}p<0.05$). Furthermore transcripts encoding HDAC-4, HDAC-7 and HDAC-9 (class II) (range n=5 and n=9 mice) were also upregulated, but not those encoding class I HDACs or DNA methyltransferases (Fig. 5b).

To verify whether the quantitative decrease of RyR1 induces alterations of the calcium release unit arrays along the muscle fiber we analyzed the intracellular distribution of RyR1 and $Ca_v1.1$ in single EDL, FDB and soleus fibers by high-resolution immunohistochemistry. The density profile of the immunofluorescence staining with anti-RyR1 Ab was not homogenous in fibers from the RyR1Q1970fsX16+A4329D mice and the changes were more pronounced in fibers isolated from EDL muscles compared to FDB and soleus muscles. In fact, EDL fibers show areas, which are randomly distributed along the longitudinal axis of the fiber, having very low, if any anti-RyR1 fluorescent signal (Fig. 6), arrow. The poor RyR1 fluorescence is specific, since the very same areas display typical triadic double row fluorescent signals with anti-$Ca_v1.1$ Ab. The apparent lack of changes of RyR1's fluorescence in FDB and soleus fibers could be due to the fact that the disarrangement of the RyR1 clusters occurs at a lower frequency in the latter muscles and/or they occur in areas of smaller dimensions.

## Electron microscopy analysis revealed a reduced calcium release units (CRU) in EDLs from RyR1Q1970fsX16+A4329D mice compared to WT.

Electron microscopy analysis showed the presence of structural alterations in muscle fibers from RyR1Q1970fsX16+A4329D mice. Adult EDL fibers from WT mice are usually characterized by regular transverse pale-dark striations (Figure 7a). Within the fiber interior mitochondria (Figure 7a, asterisks) are usually placed at the I band on both side of the Z lines next to Calcium Release Units (CRUs) or triads (Figure 7a and b and see (25, 26) for additional details). On the other hand, in EDL fibers from RyR1Q1970fsX16+A4329D mice both CRUs and mitochondria are visually less numerous (Figure 7c, asterisks). In addition CRUs morphology is often altered i.e. CRUs formed by only two elements named dyads (Figure 7d). Quantitative analysis confirmed the visual observations (Supplementary Table 4). In muscle fibers from RyR1Q1970fsX16+A4329D mice we found: (i) a significant reduction in number/100 $\mu m^2$ of CRUs (triads plus dyads; 38.2 ± 2.3 vs. 65.5 ± 1.8 in WT), mitochondria (23.0 ± 1.3 vs. 34.1 ± 1.4 in WT) and mitochondria/CRUs pairs (16.3 ± 0.9 vs. 26.4 ± 1.2 in WT); (ii) a significant increase in percentage of dyads (3.3 ± 0.7 vs 1.0 ± 0.8 in WT).

Finally RyR1Q1970fsX16+A4329D muscles showed fibers (about 18%) presenting regions (*cores*) of severe myofibrillar disorganization (Figure 7e-h). In these regions a frequent modification is the misplacement of mitochondria from the I band into clusters and/or longitudinal columns (Figure 7e, arrows). Clusters of mitochondria are always in proximity of fiber regions lacking intermyofibrillar mitochondria and CRUs (Figure 7e). Indeed in some *core* areas both mitochondria and CRUs are completely absent (Figure 7g and h).

## Calcium transients in isolated EDL and soleus muscle fibers from RyR1Q1970fsX16+A4329D heterozygous mice are significantly diminished.

The presence of the RyR1Q1970fsX16+A4329D compound heterozygous mutations causes a remarkable reduction of RyR1 protein content in skeletal muscles. In the next set of experiments we investigated whether the quantitative reduction of RyR1 protein content was accompanied by changes in $Ca^{2+}$ homeostasis. The resting $[Ca^{2+}]_i$ concentration as measured with the ratiometric $Ca^{2+}$ indicator Fura-2 in EDL, FDB and soleus fibers from RyR1Q1970fsX16+A4329D heterozygous mice was similar to that of WT littermates. The mean (±s.e.m.) resting $[Ca^{2+}]_i$ in nM was 66.26±2.60 (n=5 mice and n=43 fibers) and 67.46±2.88 (n=5 mice and n=39 fibers) for EDL, 60.33±4.74 (n=5 mice and n=45 fibers) and 62.70±2.39 (n=5 mice and n=66 fibers) for FDB and 82.14±4.42 (n=7 mice and n=29 fibers) and 80.33±3.93 (n=7 mice and n=21 fibers) for soleus in WT and RyR1Q1970fsX16+A4329D mice, respectively. In the presence of 1.8 mM $Ca^{2+}$ in the extracellular medium, the averaged peak $Ca^{2+}$ transients induced by a single action potential in EDL fibers from RyR1Q1970fsX16+A4329D heterozygous mice showed a 50% reduction compared to that observed in EDL from WT mice (0.65±0.15$^{***}$, n=40 vs 1.18±0.26, n=62, double knock-in and WT, respectively; ($\Delta F/F_0$ values are mean± S.D $^{***}p<0.005$ two-tailed Mann-Whitney test; Figure 8 and Supplementary Table 5). The peak calcium induced by an action potential in soleus and FDB fibers from RyR1Q1970fsX16+A4329D heterozygous mice were approx. 40% and 50% lower compared those of WT (for soleus 0.44±0.10$^{***}$, n=39 vs 0.65±0.22, n=33, respectively; for FDB 0.66±0.15$^{***}$ n=51 vs 1.20±0.17 n=40, respectively; $\Delta F/F_0$ values are mean± S.D., $^{***}p<0.005$ two-tailed Mann-Whitney test; Figure 8 and Supplementary Table 5). Additionally, the kinetics of the rising phase of the peak $Ca^{2+}$ transient were 15% faster in EDL fibers from RyR1Q1970fsX16+A4329D heterozygous mice compared to WT (for EDL 1.55±0.31$^{**}$ msec, n=40 vs 1.77±0.38 msec, n=62, respectively; values are mean±S.D. $p<0.01$ Mann-Whitney two tailed test). No significant differences in the kinetics of the $Ca^{2+}$ transient rising phase were observed in soleus or FDB fibers (Supplementary Table 5) (for soleus and FDB the time to peak were 2.32±0.59 n=39 vs

1.96±0.40 msec, n=33 and 1.38±0.36 msec, n= 51 vs 1.41±0.28 msec, n= 40, respectively in RyR1Q1970fsX16+A4329D and WT; values are mean±S.D.). The half relaxation time was significantly prolonged in soleus and FDB fibers from RyR1Q1970fsX16+A4329D compared to WT, whereas in EDL the half relaxation time was significantly lower (Supplementary Table 5). Furthermore, the peak $Ca^{2+}$ induced by a train of action potentials delivered at 100Hz was reduced by approximately 50%. The mean (±S.D) $\Delta F/F_0$ were 1.83±0.35 (n=22) vs $^{***}$1.02±0.27 (n=20) in EDL fibers and 1.58±0.48 (n=20) vs $^{***}$0.86±0.21 (n=25) in FDB fibers in WT and RyR1Q1970fsX16+A4329D mice, respectively (Figure 8 and Supplementary Table 5. $^{***}p<0.005$ two-tailed Mann-Whitney test). Fibers from soleus from RyR1Q1970fsX16+A4329D mice exhibited a less pronounced decrease of peak tetanic calcium transients compared to that occurring in EDL and FDB (1.26±0.32 n=29 vs 1.45±0.39 n=31, in RyR1Q1970fsX16+A4329D and WT, respectively; $\Delta F/F_0$ values are mean± S.D $^{*}p<0.05$ two-tailed Mann-Whitney test; Figure 8 and Supplementary Table 5).

## Reduced $Ca^{2+}$ sensitivity of mutant RyR1 channels.

In addition to a quantitative reduction of the RyR1 protein content, the reduced $Ca^{2+}$ transients in single fibers from compound heterozygous mice might also be linked to alterations in the conductance or gating properties of the mutant channels. We tested this hypothesis by examining single channel RyR1 function after incorporation of the skeletal muscle SR vesicles from WT and RyR1Q1970fsX16+A4329D mice into planar phospholipid bilayers. Figure 9a compares representative current fluctuations through RyR1 from WT and RyR1Q1970fsX16+A4329D mice obtained at various cytosolic free [$Ca^{2+}$] and with millimolar luminal $Ca^{2+}$ as the permeant ion. The single channel current-voltage relationship of mutant channels was similar to that of channels from WT mice (Figure 9b) yielding similar single-channel conductances (105 pS mutant and 98 pS WT), however, the sensitivity of the RyR1Q1970fsX16+A4329D channels to cytosolic $Ca^{2+}$ was severely blunted over the whole

range of [$Ca^{2+}$] tested. This can be observed in the single-channel traces (Fig. 9a) and in the Po – [$Ca^{2+}$] relationship (Figure 9c). The diminished sensitivity to activation by $Ca^{2+}$ was also confirmed by performing experiments in the presence of 1 mM caffeine and 15 μM $Ca^{2+}$. As shown in Figure 9d under these activating conditions, mutant channel activity was significantly lower compared to WT channels (Po was 0.06±0.03 and 0.30±0.03 in RyR1Q1970fsX16+A4329D and WT, respectively).

# Discussion

Here we investigated the phenotype of a compound heterozygous mouse model carrying mutations (p.Q1970fsX16+p.A4329D) in the *RYR1* gene which are isogenic with the mutations present in the *RYR1* gene of a severely affected child suffering from a recessive form of RyR1-related MmD (16, 21). The phenotype of the compound heterozygous mice recapitulates many aspects of the clinical picture of the MmD patients carrying recessive *RYR1* mutation. Indeed, the mice carrying *RYR1* compound heterozygous mutations show a 20% decrease of their body weight during the first 20 weeks after birth, a 70 % reduction of the RyR1 protein content in total homogenates from fast and slow muscles, loss of *in vivo* muscle performance and of *in vitro* muscle strength, atrophy of fast fibers especially in EDL muscles, which are associated with a deterioration of the ultrastuctural organization of the calcium release units (CRU) and the presence of cores made up by disorganized myofilaments. The recessive *RYR1* mutations are accompanied by a decrease of the peak calcium transients, an event consistent with the 70% reduction of the RyR1 protein content in sarcoplasmic reticulum membranes. In addition however, the gating of the mutant RyR1 channels is so severely affected that sensitivity to changes in cytosolic [$Ca^{2+}$] is almost abolished. This effect on RyR1 gating would also be expected to contribute to the decrease of the peak calcium transients.

To date there are no effective therapies available for congenital myopathies in general, and in particular for MmD and centronuclear myopathies, rare disorders linked to recessive

mutations in the *RYR1*. To tackle such an unmet clinical need it is important to develop animal models to test small molecules against pharmacological targets. We are confident that the RyR1Q1970fsX16+A4329D compound heterozygous mouse recapitulates most the phenotypic features of the human disease and could be exploited for preclinical studies aimed to treatment patients with congenital myopathies linked to recessive *RYR1* mutations.

Because of non-sense mediated RNA decay, the mutant allele carrying the *RYR1* Q1970fsX16 mutation of the compound heterozygous mice in not expressed (24). The consequence of such an event is (i) the monoallelic expression of the RyR1 p.A4329D missense mutation, and (ii) its quantitative reduced expression. Based on the monoallelic expression of *RYR1,* one would expect a 50% reduction of the RyR1 protein content, and yet its content in muscles from the RyR1Q1970fsX16+A4329D compound heterozygous mice only reaches approximately 30% of that present in muscles from WT mice. Although we do not have an exact explanation for the discrepancy between the real and expected RyR1 protein level in RyR1Q1970fsX16+A4329D compound heterozygous mice, we believed that the RyR1 p.A4329D missense mutation in combination with the frameshift mutation, are involved in the down-regulation of *RYR1* gene expression by several mechanisms including the induced expression of class II HDACs. This idea is consistent with data we obtained from analyzing RyR1 expression and content in RyR1Q1970fsX16 heterozygous mice (24). In the latter mouse model, the hemizygous expression of the WT *RYR1* allele is also associated with a decrease of the RyR1 protein content, nevertheless this reduction is less pronounced compared to that observed in DKI mice and did not affect the expression level of HDACs. Other explanations including a lower stability of the RyR1 p.A4329D channels may account for this, however western blots of RyR1 on muscles from the heterozygous RyR1 p.A4329D mice did not show a decrease in RyR1 content (Supplementary Figure 4).

The quantitative analysis of the CRU in muscle fibers from RyR1Q1970fsX16+A4329D mice by EM confirmed the biochemical data on the RyR1

protein expression. In fact, the EM data revealed a reduction of the number of the calcium release units (CRU) per area, and this was also accompanied by a reduction of the double strip arrays of RyR1, as indicated by the increase in the number of dyads. The most interesting results observed in the DKI mice pertain to the disarrangement of the RyR1 arrays on the junctional SR membrane which are not evenly distributed in the muscle fibers, and in such areas the RyR arrays do not exhibit the typical double strip organization. The RyR1 array disarrangements are mostly distributed along the longitudinal axis of the fast glycolytic muscles such as EDLs, whereas FDB and soleus fibers do not show evidence of such an event. Moreover, the extent of the area lacking the typical RyR1 double strip organization and their localization is irregular. The predominance of RyR1 array disarrangement in EDL compared to FDB and soleus muscles may reflect the larger fraction of the junctional SR membrane in fast fibers compared to slow oxidative fibers (27). Interestingly, the areas devoid of RyR1 array are stained with anti $Ca_v1.1$ Ab which show a typical double strip pattern. These results are consistent with the normal content of the $Ca_v1.1$ within TT membranes. The presence of the $Ca_v1.1$ in the TT membranes which are opposed to the junctional SR membrane depleted of RyR1 array suggest that, at least in the RyR1Q1970fsX16+A4329D compound heterozygous mice, the TT targeting of the $Ca_v1.1$ is independent from the targeting of the RyRs to the junctional SR membranes.

The activation of calcium release via RyR1 is due to the delivery of an orthograde signal from $Ca_v1.1$. In the last few years a great deal of data has shown that the RyR1 not only receive a signal from $Ca_v1.1$, but also generate a retrograde signal which is important for the activation of $Ca_v1.1$ $Ca^{2+}$ currents. Thus, the depletion of RyR arrays in some area of the junctional SR from DKI mice would down-regulate the retrograde signal from RyR1 to $Ca_v1.1$ which in turn would lead to a reduction of L-type $Ca^{2+}$currents via $Ca_v1.1$. If there is a direct correlation between the L-type $Ca^{2+}$currents and the RyR1 content in skeletal muscles of DKI, then one can assume a dramatic down-regulation of the $Ca^{2+}$ signaling pathways

activated by the L-type $Ca^{2+}$which are involved in the maintenance of an appropriate muscle function (28). If this were the case then the poor muscle performance of the RyR1Q1970fsX16+A4329D compound heterozygous mice might also be linked to altered $Ca_v$.1.1-mediated signaling activity, in addition to the reduction of $Ca^{2+}$release because of the marked quantitative reduction of RyR1 protein content and inability of the mutant RyR1 channels to be significantly activated by cytosolic $Ca^{2+}$.

Muscle biopsies of patients with recessive *RYR1* mutations typically show multiple minicores running along a limited length of the longitudinal axis of muscle fibers (11, 29). These minicores are areas devoid of mitochondria and do not stain with oxidative stains such NADH and cytochrome oxidase. Minicores may occur in type 1 or type 2 fibers and have a heterogeneous morphology. EM studies on human biopsies have revealed that minicores present areas of myofibrillar disorganization, sarcomeric disruption and structural changes of the sarcoplasmic reticulum and transverse tubules (29). EM analysis of the EDL from the RyR1Q1970fsX16+A4329D mice revealed the presence of areas which are structurally similar, if not identical, to the cores described in patients carrying recessive *RYR1* mutation. Although these areas are observed in 18% of the EDL a frequency which is lower compared to that described in human muscle biopsies, they retain the main ultrastructural features, namely disorganization of sarcomeric proteins, lack of calcium release units and mitochondria. We don't have an exact explanation as to why mice EDL fibers show a lower frequency of cores, but this discrepancy may be linked to species-specific differences, decreased ambulation time of the mice and/or different stages of post-natal development.

Overall comparison of the phenotype of RyR1Q1970fsX16 mice versus RyR1Q1970fsX16+A4329D mice indicates that the latter mice are more severely affected. Indeed, monoallelic RyR1 p.A4329D expression versus monoallelic WT RyR1 expression was accompanied by: (i) the presence of cores as well as a mis-alignment of RyR1 and Cav1.1 in EDL fibers; (ii) approximately 10% fewer CRU and 30% more dyads; (iii) a 30-50%

decrease in the specific force generated by isolated muscles after stimulation by a single twitch; (iv) a 36-45% decrease in the peak $Ca^{2+}$ transient elicited by electrical stimulation of soleus and EDL fibers, respectively; (v) approximately 50% shorter running distance and (vi) a 20% decrease in body weight. Interestingly, no gross changes were observed in the force generated after tetanic stimulation, nor in the peak of the $Ca^{2+}$ transients elicited by tetanic stimulation.

In conclusion the results of our study show that the phenotype of the RyR1Q1970fsX16+A4329D compound heterozygous mice largely recapitulate the clinical picture of MmD patients harboring recessive *RYR1* mutations. These results also suggest that the RyR1Q1970fsX16+A4329D compound heterozygous mouse is an animal model which can be exploited for preclinical studies aimed to treat congenital myopathies linked to recessive *RYR1* mutations.

# Materials and Methods

### Compliance with Ethical standards

All experiments involving animals were carried out on 8-12 weeks old male mice unless otherwise stated. All experimental procedures were approved by the Cantonal Veterinary Authority of Basel Stadt (BS Kantonales Veterinäramt Permit numbers 1728, 2115). All experiments were performed in accordance with relevant guidelines and regulations.

## Creation of the RyR1Q1970fsX16+A4329D compound heterozygous mice

The ex36gRNA was designed to target the following sequence in the mouse genome: aagatgcagggcaaccagcgggg (the last 3 nucleotides being the PAM sequence). Homologous recombination was achieved by using a targeting oligo encompassing the following mutated mouse genomic sequence: CAGATGTGCCACCTCCTGGAGTATTTCTGTGACCAAGAGCTGCAGCACCGGGTGG AGTCCTTGGCGGCCTTTGCAGAGTGTTATGTGGACAAGATGACAGCTGGGCAACC AGCGGGGTCGCTACGGCCTCCTCATGAAAGCCTTCACCATGAGCGCAGCCGAGAC CGCAAGGCGCACCCGAGAGTTCCGTTCTCCACCCC. To identify mutant mice a *Pvu*II restriction site flanking the mutation site was introduced (Supplementary Figure 1a).

The ex91 gRNA was designed to target the following sequence of the mouse genome: gagcagcgcggccaccgccgtgg (the last 3 nucleotides being the PAM sequence). Homologous recombination was achieved by using a gene targeting vector encompassing the following mutated mouse genomic sequence: tagttgtagcctaatctggactacttaagtcccagtctcaaaggggcctgctacaatgaaccccaccatctgctcccctcttctgcaggtg aaggagtccaagcgccagttcatcttcgacgtggtgaacgagggcggcgagtccgagaagatggagatgttcgtgagtttctgcgag gacacgatctttgagatgcagatcgcagctcagatctccgagcctgagggcgagccggaggaggacgaggacgagggcgcagag gaggctgaggagggcgcggcgggttccgacgggtcgggctctgcagcggctgcgggcgtgtgggtgtggctggcagcgactgcg

ggccgaactctacggggtctgagctaccggagcctgcggcgacgcgtgcggaggctgcggcggctgacggcgcgggaggctgct acagctgtggacgcgctgctctgggcgctggtgacccgcgcgggggcgcgggcgcgggcgcggcagccggggcgctgcggct gctctggggctcgctgtttggcggtgggctggtagacagcgccaagaaggtgacagtgacggagctcctggcaggcatgccggacc ccaccggcgacgaggtgcacggccagcagccgagcggcgctggcagcgatgcagagggcgagggtgagggagaaggcgaag gcgatgctgccgacggcgccggagatgaagaggctgcagcggaccaggctggcacgggaggtgccgacggggcggtggccgtg gcagatgggagtcccttccggccagaaggcgccggtggtctcggggatatgggtgacacgacgccagtggagccccccacgccag aaggctcgcctatcctcaagaggaagctgggggtgagagagtcctgcaaggc cloned in the *Eco*RV site of the pUC57 plasmid. To identify mutant mice a *PvuII* restriction site flanking the mutation site was introduced (Supplementary Figure 1b).

Modification of the exon36 and exon91 sequence was carried out using CRISP/Cas9 directly in fertilized mouse oocytes. C57BL/6J female mice underwent ovulation induction by i.p. injection of 5 IU equine chorionic gonadotrophin (PMSG; Folligon–InterVet), followed by i.p. injection of 5 IU human chorionic gonadotropin (Pregnyl–Essex Chemie) 48 h later. For the recovery of zygotes, C57BL/6J females were mated with males of the same strain immediately after the administration of human chorionic gonadotropin. All zygotes were collected from oviducts 24 h after the human chorionic gonadotropin injection and were then freed from any remaining cumulus cells by a 1–2 min treatment of 0.1% hyaluronidase (Sigma-Aldrich) dissolved in M2 medium (Sigma-Aldrich). Mouse embryos were cultured in M16 medium (Sigma-Aldrich) at 37°C and 5% $CO_2$. For micromanipulation, embryos were transferred into M2 medium. All microinjections were performed using a microinjection system comprised of an inverted microscope equipped with Nomarski optics (Nikon), a set of micromanipulators (Narashige), and a FemtoJet microinjection unit (Eppendorf). Injection solution containing sgRNA (300ng/µl), Cas9 mRNA (100ng/µl) Cas9 protein (50ng/µl) and homologous recombination template (ssDNA oligonucleotide for ex36 or plasmid ex91, respectively) (10 ng/µl) was microinjected into the male pronuclei of fertilized mouse oocytes until 20-30% distension of the organelle was observed.

Embryos that survived the microinjection were transferred on the same day into the oviducts of 8–16-wk-old pseudopregnant Crl:CD1 (ICR) females (0.5 d used after coitus) that had been mated with sterile genetically vasectomized males (30) the day before embryo transfer. Pregnant females were allowed to deliver and raise their pups until weaning age.

The single RyR1Q1970fsX16 and RyR1A4329D heterozygous *RYR1* mice were intercrossed to obtain RyR1Q1970fsX16+A4329D compound heterozygous double knock in (DKI) mice, which represented 20-25% of the littermates, indicating a Mendelian transmission of each mutant allele.

## Genotyping RyR1Q1970fsX16+A4329D mice and real time qPCR

PCR amplification of *RYR1* exon 36 and exon 91 was performed as previously described (24) on genomic DNA of WT and RyR1Q1970fsX16+A4329D mutant mice using specifically designed primers (Supplementary Table 1). GoTaq® DNA Polymerase (Promega) was used in the amplification of the product. Briefly, reactions were performed using the following conditions: for exon 36 the PCR was initiated with a 5 min. at 95°C, followed by 30 cycles of 95°C for 30 s, 59°C for 30 s, and 72°C for 30 s, and final extension step at 72°C for 7 min. For exon 91 the PCR was initiated with a 10 min. hold at 94°C followed by 35 cycles of 98°C for 10 s, 62°C for 30 s, and 72°C for 90 s, and final extension step at 72°C for 5 min. The amplified DNA products were digested with *PvuII* (R0151L BioLabs) for 1 hour at 37°C, separated on a 7.5% polyacrylamide gel and stained with ethidium bromide to visualize DNA bands. PCR products were also purified using the QIAquick PCR-purification kit 250 (QIAGEN) according to the manufacturer's instructions, and were directly sequenced, in forward and reverse directions with Microsynth Sanger Sequencing method. For quantitative real-time polymerase chain reaction (qPCR), cDNA was prepared from total RNA extracted from frozen hind limb muscles using TRIzol® (ThermoFischer; 15596026) according to the

manufacturer's instructions. DNA was removed using DNase I (Invitrogen; 18068-015) and 1000 ng RNA were reverse-transcribed into cDNA using the High capacity cDNA Reverse Transcription Kit (Applied Biosystems; 4368814). The cDNA was amplified by qPCR using the primers listed in Supplementary Table 1 and transcript levels were quantified using Power SYBR® Green reagent Master Mix (Applied Biosystems; 4367659), using the Applied Biosystems 7500 Fast Real-time PCR System running 7500 software version 2.3. Transcript quantification was based on the comparative ΔΔCt method. Each reaction was performed in duplicate and results are expressed as relative gene expression normalized to desmin (DES).

## *In Vivo* Muscle Strength Assessment

Mice were individually housed in cages equipped with a running wheel carrying a magnet as previously described (31). Wheel revolutions were registered by reed sensors connected to an I-7053D Digital-Input module (Spectra), and the revolution counters were read by a standard laptop computer via an I-7520 RS-485-to-RS-232 interface converter (Spectra). Digitized signals were processed by the ''mouse running'' software developed at Santhera Pharmaceuticals. Total running distance (meter) and speed (Km/h) were evaluated.

## *In Vitro* Muscle Strength Assessment

To test muscle force *in vitro*, (WT and RyR1Q1970fsX16+A4329D) *extensor digitorum longus* (EDL) and soleus muscles were dissected from 12 weeks old mice and mounted onto a muscle force transducing setup (Heidelberg Scientific Instruments) as previously described (31). Muscle force was digitized at 4 kHz by using an AD Instrument converter and stimulated with 15 V pulses for 1.0 msec. EDL tetanus was recorded in response to a train of pulses of 400 msec and 1100 msec duration delivered at 10/20/50/100/150 Hz, and 10/20/50/100/120 Hz, for EDL and Soleus, respectively. Specific force was normalized to the muscle cross-sectional area [CSA_wet weight (mg)/length (mm)_1.06 (density mg/mm$^3$)].

## Quantitative analyses by EM

Data were collected from three months-old WT (n=2 mice) and RyR1Q1970fsX16+A4329D (n=2 mice) EDL muscles. In each sample, 20 fibres were analysed. In each fibre 2-3 micrographs (all at the same magnification, 14K, and of non-overlapping regions) were randomly collected from longitudinal sections. CRUs and mitochondria were marked and counted in each micrograph. The number of CRUs/area, mitochondria/area and mitochondria-CRUs pairs/area is reported as an average number /100 $\mu m^2$ (25). In each EM image, we also determined: (i) the mitochondrial positioning with respect to the I and A bands. If an individual mitochondrion extended from one I band to another, it was counted in both; (ii) the number of dyads i.e. incomplete triads expressed as percentages over the total number of CRUs. Note: in RyR1Q1970fsX16+A4329D muscle fibers there was a consistent percentage of fibers (about 18%) presenting regions (*cores*) of severe myofibrillar disorganization: the EM quantification was performed only on the apparently normal regions.

## Isolation of single fibers from EDL, FDB and soleus muscles

animals 6-7 weeks of age were killed by pentobarbital overdose according to procedures approved by the local animal care committee. Mouse hearts were exposed and washed with an injection of Tyrode's normal mammalian Ringer buffer (137 mM NaCl, 5.4 mM KCl, 0.5 mM $MgCl_2$, 1.8 mM $CaCl_2$, 0.1% glucose, 11.8 mM HEPES, pH 7.4 NaOH), followed by an injection of premix; 0.1% Collagenase type I (Clostridium hystoliticum Type I, Sigma-Aldrich), 0.08% Collagenase type II (Clostridium hystoliticum Worthington biochemical corporation) and 0.05% Elastase (porcine pancreas Worthington biochemical corporation) diluted in Tyrode's buffer. Following the washing steps, EDL FDB, and soleus muscles were isolated and digested with 0.2% of Collagenase type I (Clostridium hystoliticum Type I, Sigma-Aldrich) and 0.2% of Collagenase type II (Clostridium hystoliticum Type II,

Worthington) in Tyrode's buffer for 45 minutes at 37 °C 5% $CO_2$ for *flexor digitorum brevis* (FDB) muscles, 50 minutes for EDL muscles and 55 minutes for soleus muscles. The muscles were washed with Tyrode's buffer to block the collagenase activity, and gently separated from tendons using large to narrowest set of fire-polished Pasteur pipettes. Fibers obtained by this procedure remained excitable and contracted briskly when assayed experimentally. Finally, fibers were placed either on 35 mm glass bottom dishes (MatTek corporation) for measurements of the resting [$Ca^{2+}$] or on ibiTreat 15µ-Slide 4 well (Ibidi), previously coated with 5 µl (1 mg/ml) of laminin (ThermoFischer, 23017015) and placed in the incubator for 1 hour to settle down. The fibers were then used for electrically evoked measurements of the $Ca^{2+}$ transients and for immunohistochemistry.

## Resting [$Ca^{2+}$] measurements

Single EDL, FDB and soleus fibers were isolated from 5-7 mice and plated on a 35 mm glass bottom dishes (MatTek corporation) coated with 5 µl (1 mg/ml) of laminin (ThermoFischer). The fibers were incubated for 20 min at 20°C in normal mammalian Ringer's buffer (137 mM NaCl, 5.4 mM KCl, 0.5 mM $MgCl_2$, 1.8 mM $CaCl_2$, 0.1% glucose, 11.8 mM HEPES, pH 7.4 NaOH) containing 5 µM Fura-2, AM (Invitrogen). The excess fura-2 was diluted out by the addition of fresh Ringer's solution and measurements of the resting [$Ca^{2+}$] were carried out as previously described (32), using an inverted Zeiss Axiovert fluorescent microscope. Only those fibers that contracted when an electrical stimulus was applied were used for the [$Ca^{2+}$] measurements.

## Electrically evoked $Ca^{2+}$ transients

Single EDL, FDB and soleus fibers were incubated for 10 min at 19 °C in Ringer's solution containing 10 µM low affinity calcium indicator Mag-Fluo-4 AM (ThermoFischer), 50 µM N-benzyl-p-toluene sulfonamide (BTS, Tocris). Fibers were rinsed twice with fresh Tyrode's

solution, and measurements were carried out in Tyrode's solution containing 50 μM BTS. Measurements were carried out with a Nikon Eclipse inverted fluorescent microscope equipped with a 20x PH1 DL magnification objective. The light signals from a spot of 1 mm diameter of the magnified image of FDB, EDL and soleus fibers were converted into electrical signals by a photomultiplier connected to a Nikon Photometer P101 amplifier. Fluorescent signals were acquired using a custom-designed software (RCS AUTOLAB) and analyzed by PowerLab Chart5 and Origin.6 programs. Changes in fluorescence were calculated as $\Delta F/F_{0=}$ $(F_{max}- F_{rest})/(F_{rest})$. Kinetic parameters were analyzed using Chart5 software. Fibers were excited at 480 nm and then stimulated either with a single pulse of 50 V with a duration of 1 msec, or with a train of pulses of 50 V with a duration of 300 msec delivered at 100 Hz. Fibers were isolated from 3-5 mice.

## Immunostaining

Single EDL, FDB and soleus fibers were isolated from 6/7 weeks old WT and RyR1Q1970fsX16+A4329D mice. The fibers were fixed in 4% paraformaldehyde for 30 minutes at room temperature, followed by free aldehyde group quenching with 0.1 M glycine for 10 minutes at room temperature. The fibers were then permeabilized with 1% Triton X-100 in PBS for 30 minutes at 37°C and non-specific binding sites were blocked with 1% blocking buffer (Roche catalogue N°11500694001) in PBS for 1 hour at room temperature. After washing the fibers were incubated with the primary antibodies, RyR1 (Cell Signaling) (1:50) and $Ca_v1.1$ (Developmental Studies Hybridoma Bank) (1:5), overnight at 4°C. Fibers were then incubated for 60 min at room temperature with the appropriate Alexa Fluor conjugated secondary antibody (chicken anti-rabbit and donkey anti-mouse conjugated Alexa-Fluor 488 and Alexa-Fluor 568 respectively; Thermo Fischer). Nuclei were counterstained with 4',6-diamino-2-phanylindole (DAPI)(ThermoFischer Scientific). Fibers were observed with a Nikon A1plus confocal microscope equipped with Nikon Plan Apo 60x oil objective

(NA 1.4) and with Coherent® Sapphire lasers (488 and 561 nm) and an MPBC®CW Visible Fiber laser (647 nm) controlled by Nikon® NIS-Elements Confocal software (version 4.6).

## Histological examination

EDL and soleus muscles from RyR1Q1970fsX16+A4329D and WT mice were isolated and mounted for fluorescence microscopy imaging. Changes in muscle fiber type and calculation of the minimal Feret diameter, the closest possible distance between the two parallel tangents of an object, were determined as described (33). Images were obtained using an Olympus IX series microscope and analyzed using the CellP Software.

## Biochemical analysis of total muscle homogenates

Total muscle homogenates were prepared from EDL and soleus muscles of WT and RyR1Q1970fsX16+A4329D mice. SDS-polyacrylamide electrophoresis and Western blots of total homogenates were carried out as previously described (20, 32). Western blots were stained with the primary antibodies listed in Supplementary Table 2, followed by peroxidase-conjugated Protein G (Sigma P8170; 1:130'000) or peroxidase-conjugated anti-mouse IgG (Fab Specific) Ab (Sigma A2304; 1:200'000). The immuno-positive bands were visualized by chemiluminescence using the WesternBright ECL- HRP Substrate (Witec AG). Densitometry of the immune-positive bands was carried out using the Fusion Solo S (Witec AG). A representative immunoblot of each antibody on total muscle homogenates from WT mice is shown in Supplementary Figure 2.

## Single channel recordings

Mouse skeletal membrane fractions were prepared as described previously (34) from WT and RyR1Q1970fsX16+A4329D mice aged 8-12 weeks. RyR1 channels were incorporated into planar phosphatidylethanolamine lipid bilayers as previously described (35) and current

fluctuations through RyR1 channels were recorded under voltage-clamp conditions with 250 mM HEPES, 80 mM Tris, 5 μM free $Ca^{2+}$, pH 7.2, and 250 mM glutamic acid, 10 mM HEPES, pH to 7.2 with $Ca(OH)_2$ (free [$Ca^{2+}$] approximately 50 mM) on the *trans* (luminal) side of the bilayer at 21°C. The *trans* chamber was voltage-clamped at ground. The free [$Ca^{2+}$] and pH of the solutions were maintained constant during the experiment and were determined using a $Ca^{2+}$ electrode (Orion 93-20, Thermo Fisher Scientific, UK) and a Ross-type pH electrode (Orion 81-55, Thermo Fisher Scientific, UK) as previously described [28]. Free cytosolic $Ca^{2+}$ levels were increased by additions of $CaCl_2$.

## Single-channel analysis

Single-channel recordings were digitized at 20 kHz and low-pass filtered at 800 Hz. Open probability (Po) was determined over 3 min of continuous recording at 0 mV using 50% threshold analysis (36) in Clampfit 10.6 (Molecular Devices, USA) as previously described (37). Where Po values are shown in figures, the Po above each trace refers to the value determined over 3 min for that particular channel. Where more than one channel incorporated into the bilayer, Po is reported as an average (total Po divided by number of channels).

## Statistical Analysis

Statistical analysis was performed using the Student's unpaired *t* test for normally distributed values and the Mann–Whitney U test when values were not normally distributed. $p<0.05$ was considered significant. For the single channel recordings a two-way ANOVA with a within subjects factor ([$Ca^{2+}$]) and between subjects factor (genotype) was performed. We first checked for statistical significance for the interaction of the two independent variables ([$Ca^{2+}$] and genotype) and then for main effects for each of the two independent variables. The interaction between [$Ca^{2+}$] and genotype was found to be statistically significant ($P = 0.011$).

There were also significant main effects of [$Ca^{2+}$] (P = 0.007) and genotype (p<0.0001). Performing multiple comparisons tests with Sidak's correction showed that there was also a statistically significant difference between the response of WT and RyR1Q1970fsX16+A4329D mice at 100 μM $Ca^{2+}$ (p< 0.0001).

## Acknowledgements

This work was supported by a grant from the Swiss National Science Foundation (SNF N° 31003A-169316), a grant from the BOTNAR Stiftung, a grant from the OPO-Stiftung, a grant from the Swiss muscle foundation (FSRMM), a grant from NeRAB, and a grant from M.I.U.R. P.R.I.N. 2015. The support of the Department of Anesthesia Basel University Hospital is gratefully acknowledged. We would like to thank Heide Oller and Anne-Sylvie Monnet for expert technical assistance and support.

## Conflict of interests

The authors declare that they have no conflict of interests.

# References


1. Rios, E. and Pizarro, G. (1991). Voltage sensor of excitation-contraction coupling in skeletal muscle. *Physiol. Rev.,* **71,** 849-908.
2. Endo, M. (1977). Calcium release from the sarcoplasmic reticulum. *Physiol. R*ev., **57**, 71-108.
3. Fleischer, S. and Inui, M. (1989). Biochemistry and biophysics of excitation-contraction coupling. *Annu. Rev. Biophys. Biophys. Chem*., **18**, 333-364.
4. MacLennan, D. H. (2000). $Ca^{2+}$ signaling and muscle disease. *Eur. J. Biochem*., **267**, 5291-5297.
5. Franzini-Armstrong, C. and Jorgensen, A. (1994). Structure and development of E-C coupling units in skeletal muscle *Annu. Rev. Physiol*., **56**, 509-534.
6. Calderon, J. C., Bolanos, P. and Caputo, C. (2014). The excitation-contraction coupling mechanism in skeletal muscle. *Biophys. Rev*., **6**, 133-160.
7. Treves, S., Vukcevic, M., Maj, M., Thurnheer, R., Mosca, B. and Zorzato, F. (2009). Minor sarcoplasmic reticulum membrane components that modulate excitation-contraction coupling in striated muscles. *J. Physiol*., **587**, 3071-3079.
8. Nakai, J., Dirksen, R. T., Nguyen, H. T., Pessah, I. N., Beam, K. G. and Allen, P. D. (1996). Enhanced dihydropyridine receptor channel activity in the presence of ryanodine receptor. *Nature,* **380**, 72-75.
9. Andronache, Z., Hamilton, S. L., Dirksen, R. T. and Melzer, W. (2009). A retrograde signal from RyR1 alters DHP receptor inactivation and limits window $Ca^{2+}$ release in muscle fibers of Y522S RyR1 knock in mice. *Proc. Natl. Acd. Sci. U.S.A*., **106**, 4531-4536.
10. Meissner, G. (2017). The structural basis of ryanodine receptor ion channel function. *J. Gen. Physiol.,* **149**, 1065-1089.

11. Jungbluth, H., Treves, S., Zorzato, F., Sarkozy, A., Ochala, J., Sewry, C., Phadke, R., Gautel, M. and Muntoni, F. (2018). Congenital myopathies: disorders of excitation-contraction coupling and muscle contraction. *Nat. Rev. Neurol*., **14**, 151-167.

12. Rossignol, B., Gueret, G., Pennec, J. P., Morel, J., Rannou, F., Giroux-Metges, M. A., Talarmin, H., Gioux, M. and Arvieux, C. C. (2008). Effects of chronic sepsis on contractile properties of fast twitch muscle in an experimental model of critical illness neuromyopathy in the rat. *Crit. Care Med*., **36**, 1855-1863.

13. Friedrich, O. (2006). Critical illness myopathy: what is happening? *Curr. Opin. Clin. Nutr. Metab. Care,* **9**, 403-409.

14. Treves, S., Jungbluth, H., Muntoni, F. and Zorzato, F. (2008). Congenital muscle disorders with cores: the ryanodine receptor calcium channel paradigm. *Curr. Opin. Pharmacol*., **8**, 319-326.

15. Monnier, N*.,* Marty, I., Faure, J., Castiglioni, C., Desnuelle, C., Sacconi, S., Estournet, B., Ferreiro, A., Romero, N., Laquerriere, A., *et al.* (2008). Null mutations causing depletion of the type 1 ryanodine receptor (RYR1) are commonly associated with recessive structural congenital myopathies. *Hum. Mutat*., **29**, 670-678.

16. Zhou, H., Jungbluth, H., Sewry, C. A., Feng, L., Bertini, E., Bushby, K., Straub, V., Roper, H., Rose, M. R., Brockington, M., *et al.* (2007). Molecular mechanisms and phenotypic variation in RYR1-related congenital myopathies. *Brain,* **130**, 2024-2036

17. Wilmshurst, J. M., Lillis, S., Zhou, H., Pillay, K., Henderson, H., Kress, W., Müller, C. R., Ndondo, A., Cloke, V., Cullup, T., *et al*. (2010). RYR1 mutations are a common cause of congenital myopathies with central nuclei. *Ann. Neurol*., **68**, 717-726.

18. Zhou, H. Rokach, O., Feng, L., Munteanu, I., Mamchaoui, K., Wilmshurst, J. M., Sewry, C., Manzur, A. Y., Pillay, K., Mouly, V., *et al.* (2013). RYR1 deficiency in

congenital myopathies disrupts excitation-contraction coupling. *Hum. Mutat*., **34**, 986–996.

19. Zhou, H., Brockington, M., Jungbluth, H., Monk, D., Stanier, P., Sewry, C. A., Moore, G. E. and Muntoni, F. (2006). Epigenetic allele silencing unveils recessive RYR1 mutations in core myopathies. *Am. J. Hum. Genet*., **79,** 859-968.
20. Rokach, O., Sekulic-Jablanovic, M., Voermans, N., Wilmshurst, J., Pillay, K., Heytens, L., Zhou, H., Muntoni, F., Gautel, M., Nevo, Y., *et al.* (2015). Epigenetic changes as a common trigger of muscle weakness in congenital myopathies. *Hum. Mol. Genet*., **24**, 4636-4647.
21. Klein, A., Lillis, S., Munteanu, I., Scoto, M., Zhou, H., Quinlivan, R., Straub, V., Manzur, A.Y., Roper, H., Jeannet, P. Y., *et al*. (2012). Clinical and genetic findings in a large cohort of patients with ryanodine receptor 1 gene-associated myopathies. *Hum. Mutat*., **33**, 981-988.
22. Schiaffino, S. and Reggiani, C. (2011). Fiber types in mammalian skeletal muscles. *Physiol. Rev.,* **91**, 1447-1531.
23. Calderón, J.C., Bolaños, P. and Caputo, C. (2009). Myosin heavy chain isoform composition and $Ca^{2+}$ transients in fibres from enzymatically dissociated murine soleus and extensor digitorum longus muscles. *J. Physiol*., **588**, 267-279.
24. Elbaz, M., Ruiz, A., Eckhardt, J., Pelczar, P., Muntoni, F., Boncompagni, S., Treves, S. and Zorzato, F. (2019). Quantitative reduction of RyR1 protein caused by a single-allele frameshift mutation in *RYR1* ex36 impairs the strength of adult skeletal muscle fibres. *Hum. Mol. Genet*., doi: 10.1093/hmg/ddz025.
25. Boncompagni, S., Rossi, A. E., Micaroni, M., Beznoussenko, G. V., Polishchuk, R. S., Dirksen, R. T. and Protasi, F. (2009). Mitochondria are linked to calcium stores in striated muscle by developmentally regulated tethering. *Mol. Biol. Cell.,* **20**, 1058-1067.

26. Pietrangelo, L., D' Incecco, A., Ainbinder, A., Michelucci, A., Kern, H., Dirksen, R. T., Boncompagni, S. and Protasi, F. (2015). Age-dependent uncoupling of mitochondria from $Ca^{2+}$ release units in skeletal muscle. *Oncotarget*., **6** (34): 35358-71. doi: 10.18632/oncotarget.6139.

27. Eisenberg, B. R. and Salmons, S. (1981). The reorganization of subcellular structure in muscle undergoing fast-to-slow type transformation. A stereological study. *Cell Tissue Res*., **220**, 449-471.

28. Lee, C. S., Dagnino-Acosta, A., Yarotskyy, V., Hanna, A., Lyfenko, A., Knoblauch, M., Georgiou, D. K., Poché, R. A., Swank, M. W., Long, C., *et al*. (2015). $Ca^{2+}$ permeation and/or binding to Cav1.1 fine-tunes skeletal muscle $Ca^{2+}$ signaling to sustain muscle function. *Skelet. Muscle,* **5**:4 doi: 10.1186/s13395-014-0027-1.

29. Jungbluth, H. (2007). Multi-mnicore disease. *Orphanet. J. Rare. Dis*., **2**:31 doi: 10.1186/1750-1172-2-31 .

30. Haueter, S., Kawasumi, M., Asner, I., Brykczynska, U., Cinelli, P., Moisyadi, S., Bürki, K., Peters, A. H. and Pelczar, P. (2010). Genetic vasectomy-overexpression of Prm1-EGFP fusion protein in elongating spermatids causes dominant male sterility in mice. *Genesis,* **48**, 151-160.

31. Mosca, B., Delbono, O., Messi, L. M., Bergamelli, L., Wang, Z. M., Vukcevic, M., Lopez, R., Treves, S., Nishi, M., Takeshima, H., *et al*. (2013). Enhanced dihydropyridine receptor calcium channel activity restores muscle strength in JP45/CASQ1 double knockout mice. *Nat. Commun*., **4:** 1541. doi: 10.1038/ncomms2496.

32. Bachmann, C., Jungbluth, H., Muntoni, F., Manzur, A. Y., Zorzato, F. and Treves, S. (2016). Cellular, biochemical and molecular changes in muscles from patients with X-linked myotubular myopathy due to MTM1 mutations. *Hum. Mol. Genet*., **26**, 320-332

33. Briguet, A., Courdier-Fruh, I., Foster, M., Meier, T. and Magyar, J. P. (2004). Histological parameters for the quantitative assessment of muscular dystrophy in the mdx-mouse. *Neuromuscul. Disord*., **14**, 675-682.

34. El-Ajouz, S., Venturi, E., Witschas, K., Beech, M., Wilson, A. D., Lindsay, C., Eberhardt, D., O'Brien, F., Iida, T., Nishi, M., *et al.* (2017). Dampened activity of ryanodine receptor channels in mutant skeletal muscle lacking TRIC-A. *J. Physiol.,* **595**, 4769-4784

35. Sitsapesan, R., Montgomery, R. A., MacLeod, K. T. and Williams, A. J. (1991). Sheep cardiac sarcoplasmic reticulum calcium-release channels: modification of conductance and gating by temperature. *J. Physiol*., **434**, 469-488,

36. Colquhoun, D. and Sigworth, F. J. (1995). Fitting and Statistical Analysis of Single-Channel Records. In Sakmann B and Neher E (eds) Single-Channel Recording, Springer US Boston, MA, pp. 483–587

37. Venturi, E., Galfré, E., O'Brien, F., Pitt, S. J., Bellamy, S., Sessions, R. B. and Sitsapesan, R. (2014). FKBP12.6 activates RyR1: investigating the amino acid residues critical for channel modulation. *Biophys. J*., **106**, 824-833.

**Figure 1.** The body weight of RyR1Q1970fsX16+A4329D heterozygous mice is significantly diminished starting 3 weeks after birth. **(a)** E17 RyR1Q1970fsX16+A4329D embryos are undistinguishable from WT or single *RYR1* heterozygous mutant littermates. **(b)** RyR1Q1970fsX16+A4329D mice at 8 weeks are visibly smaller than their WT littermates. The picture shows a male WT mouse (bottom) and a RyR1Q1970fsX16+A4329D mouse (top). **(c)** Body weight growth curves of female and male WT (filled squares, continuous line) and RyR1Q1970fsX16+A4329D (filled triangles, dashed line) monitored during a period of 16 weeks. Each symbol shows the average (±S.D.) weight of n=11-13 mice. $p<0.05$ Mann-Whitney two tailed test, for time points after 3 weeks of age.

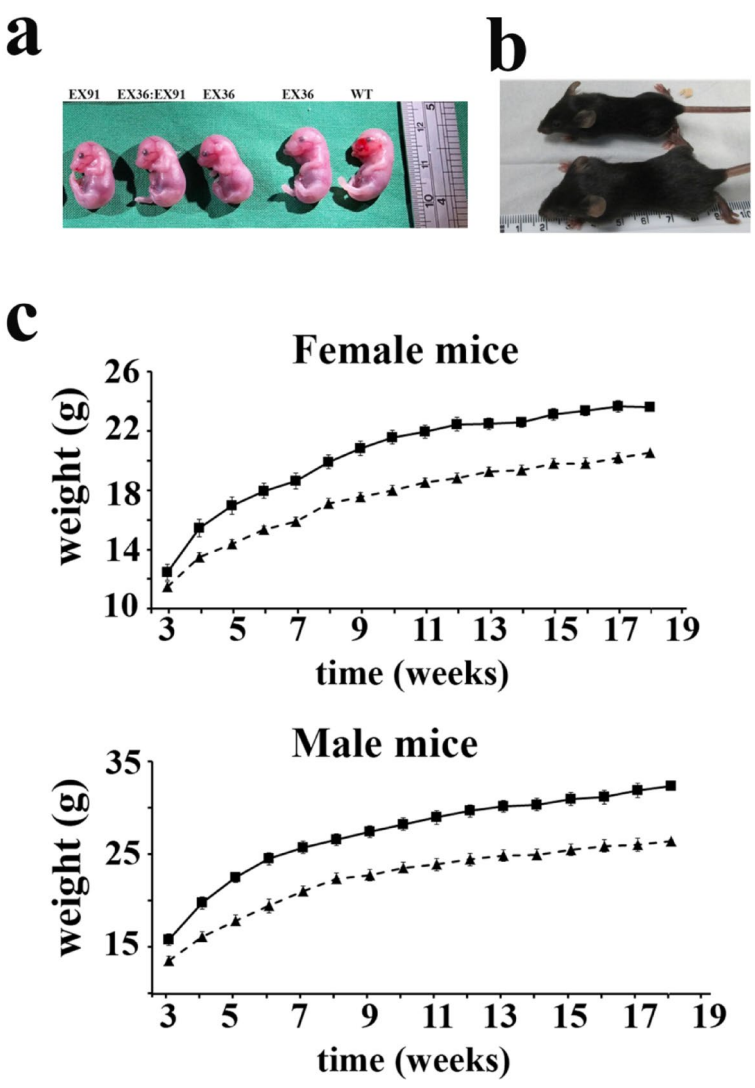

**Figure 2**. RyR1Q1970fsX16+A4329D mice show diminished *in vivo* muscle function as assessed using the voluntary running wheel. **(a)** Total running distance and **(b)** total running speed. Spontaneous running activity was measured for 21 days in individually housed 12-weeks-old WT (filled squares, continuous line) and RyR1Q1970fsX16+A4329D (filled triangles squares, dashed line) mice during the dark-phase. Each cage was equipped with a running wheel. Each symbol represents the mean ± SEM (n=9 WT and n=7 RyR1Q1970fsX16+A4329D mice). $p \leq 0.05$ (Mann–Whitney two-tailed test).

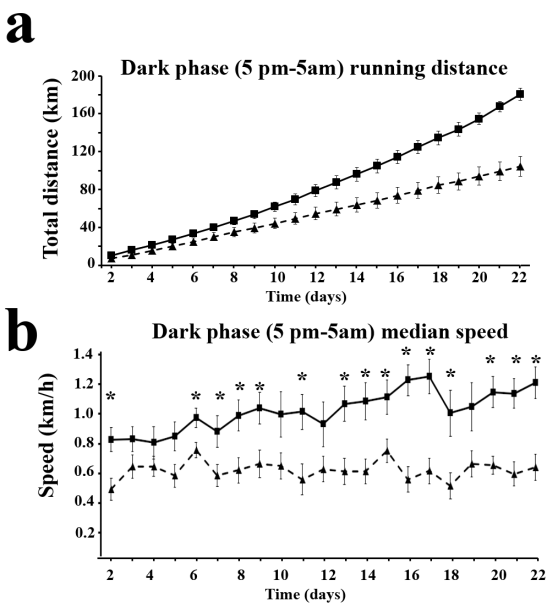

**Figure 3**. Mechanical properties of EDL and soleus muscle from WT RyR1Q1970fsX16+A4329D mice. **(a)** and **(b)** show representative traces of single twitches. **(c)** and **(d)** show representative traces of maximal tetanic forces in EDL and soleus muscles isolated from WT (continuous line) and RyR1Q1970fsX16+A4329D mice (dotted line). **(e)** and **(f)** Whisker plots of tetanic force generated by isolated muscles from WT and RyR1Q1970fsX16+A4329D mice electrically stimulated at 50 Hz, 100 Hz and 150 Hz (EDL muscles) and electrically stimulated at 50 Hz, 100 Hz and 120 Hz (soleus muscles). Each symbol represents the value from a single mouse. $^{**}p \leq 0.01$ (Mann–Whitney two-tailed test).

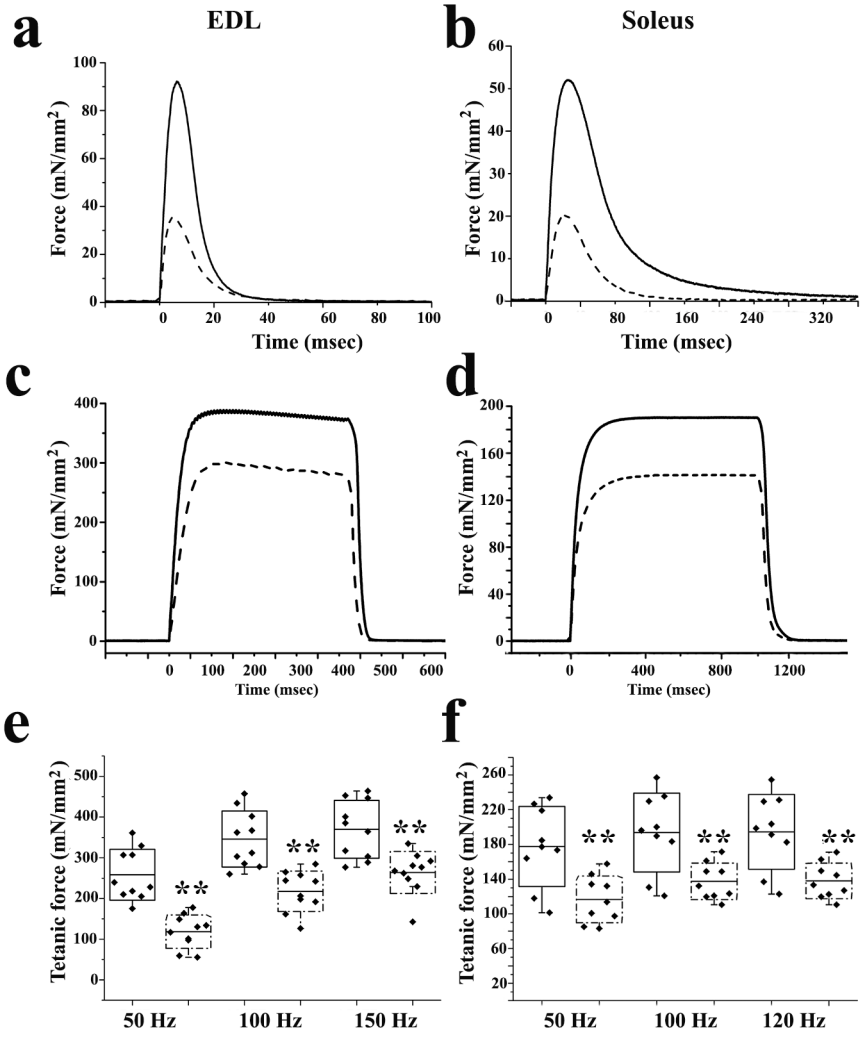

**Figure 4.** EDL muscles from RyR1Q1970fsX16+A4329D mice are atrophic. **(a)** EDL and soleus muscles were sectioned with a cryostat, stained with anti-laminin and anti-MyHC I Ab, imaged with an inverted fluorescent microscope and analyzed as described in the Methods section. Bar indicates 200 µm. (**b)** Quantification of the fiber type composition of soleus (left panel) and EDL (right panel) muscles from WT (black bars) and RyR1Q1970fsX16+A4329D mice (white bars). Values are presented as mean (± s.e.m.) % fibers. (**c)** Minimal Feret fiber distribution. Measurements were carried out on cross sections of soleus (left) and EDL (right) muscles from WT (black squares, continuous line) and RyR1Q1970fsX16+A4329D (black triangles, dashed line). WT soleus= 3144 fibers, RyR1Q1970fsX16+A4329D soleus =3392 fibers, WT EDL= 2232 fibers and RyR1Q1970fsX16+A4329D EDL= 3415 fibers, (n=2 mice per genotype). Data points are expressed as mean ± s.e.m.

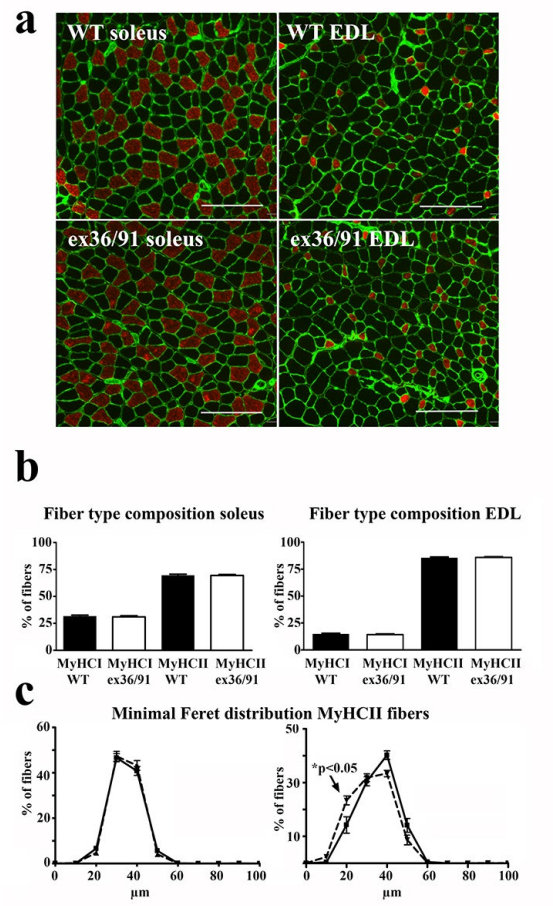

**Figure 5.** RyR1 protein and transcript levels are decreased in muscles from RyR1Q1970fsX16+A4329D mice. **(a)** Biochemical characterization of total homogenates of EDL and soleus muscles from WT and RyR1Q1970fsX16+A4329D mice. Left panels show representative immunoblots probed with the indicated antibodies. Right panels show % content of the indicated proteins in EDL (top) and soleus (bottom) muscles. Whisker plots represents the values from n=9-10 mice; a minimum of 3 repeats were done for each data point. The intensity values obtained from WT mice were considered 100%. (**b)** Quantitative real-time PCR (RT-qPCR) of the indicated transcripts in skeletal muscles from RyR1Q1970fsX16+A4329D mice relative to WT mice (the latter were set as 1). Transcript levels were normalized to DES as a muscle specific gene using the ΔΔCt method. $^{*}p<0.05$; $^{***}p<0.005$; $^{****}p<0.001$ (Mann–Whitney two-tailed test).

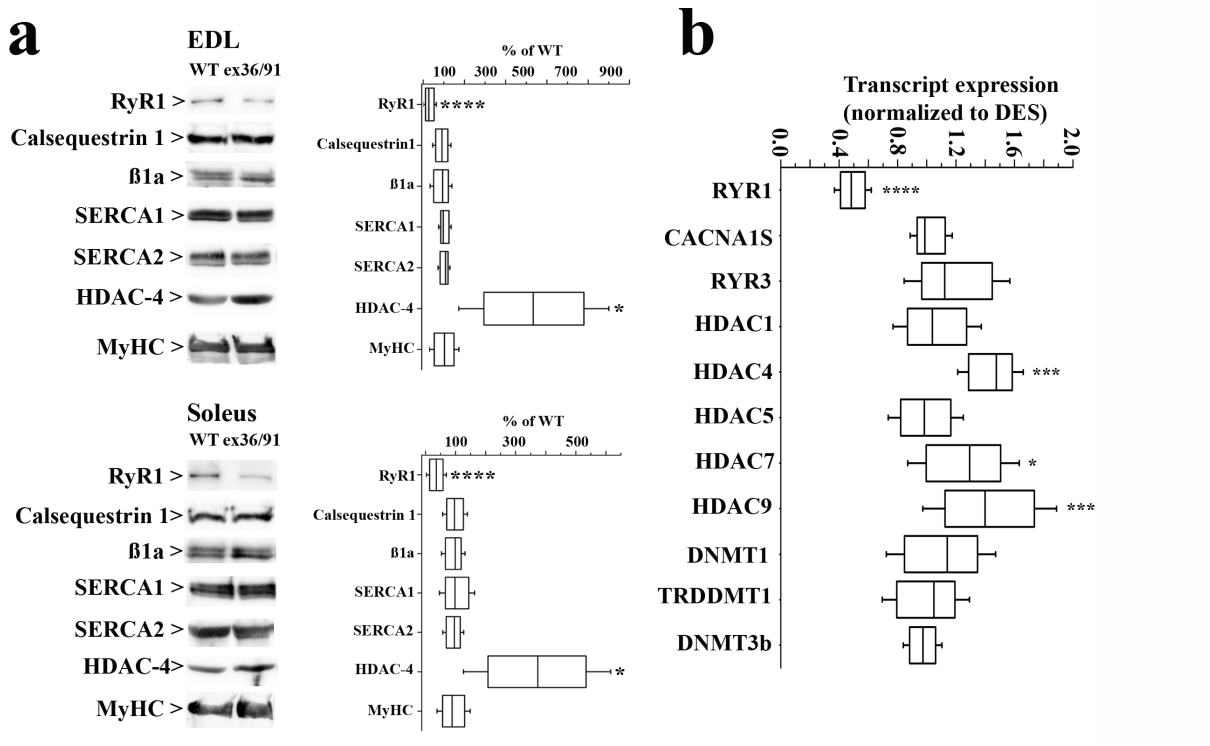

**Figure 6**. The organization of the sarcoplasmic reticulum is disrupted in muscle fibers from RyR1Q1970fsX16+A4329D mice. Left panels show representative confocal images of EDL, FDB and soleus fibers labeled with anti-RyR1 (green), anti-$Ca_v1.1$ (red) antibodies and merged images. Bar =10 µm. Right panels show intensity profile plots for RyR1 and $Ca_v1.1$ distribution. The intensity profile of RyR1 is visibly disrupted in the EDL muscle from the RyR1Q1970fsX16+A4329D mice. Experiments were carried out on fibers isolated from 3 WT and 4 RyR1Q1970fsX16+A4329D mice. Images of EDLs were from 32 WT and 36 RyR1Q1970fsX16+A4329D fibers (9 fields per fiber). Images of FDBs were from 31 WT and from 32 RyR1Q1970fsX16+A4329D fibers (6-9 fields per fiber). Images from soleus were from 24 WT and 30 RyR1Q1970fsX16+A4329D fibers (9 fields per fiber).

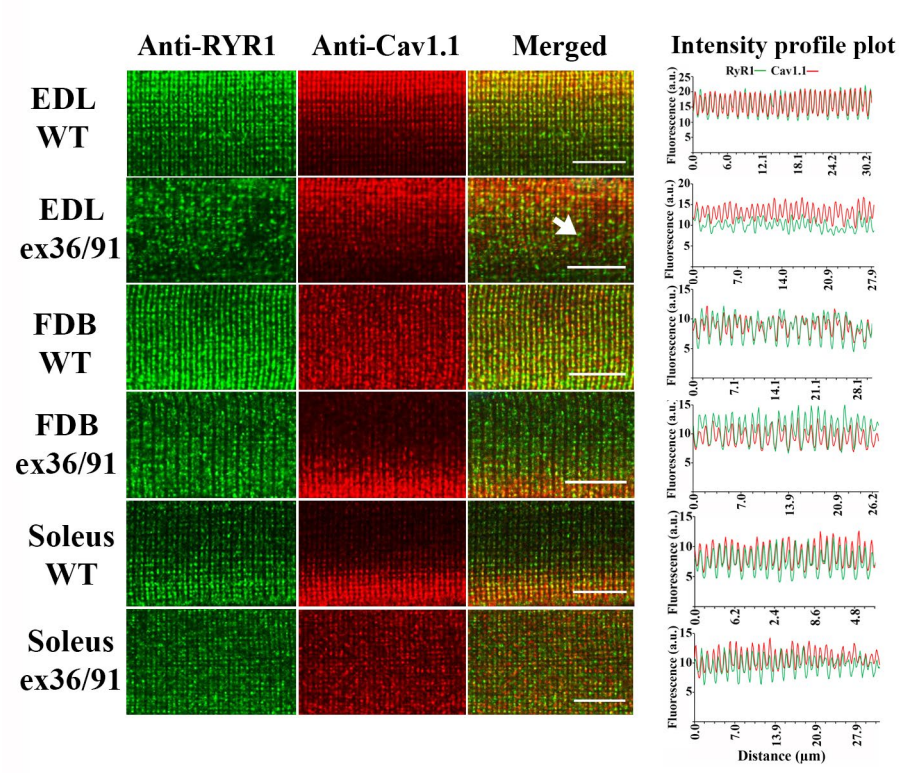

**Figure 7.** Ultrastructure of EDL from WT and RyR1Q1970fsX16+A4329D mice. **(a)** In adult WT EDL fibers mitochondria are usually placed at the I band in proximity of Z lines (asterisks), next to CRUs. CRUs are mostly in the form of triads: two SR vesicles closely opposed to a central T-tubule **(b). (c)** In EDL fibers from RyR1Q1970fsX16+A4329D mice, mitochondria are visually less abundant and CRUs are often found in the form of dyads **(d)**. **(e)** In some fibers from RyR1Q1970fsX16+A4329D mice mitochondria are misplaced from their correct triadic position forming clusters between the myofibrils (arrows). Relocation of mitochondria leaves areas where mitochondria and CRUs are almost completely absent **(f)**. **(g)** Cross section of a fiber from RyR1Q1970fsX16+A4329D muscle showing a *core* region: degenerated area characterized by total disruption of the myofibrillar organization. Within the *core* region CRUs and mitochondria are completely absent **(h)**. Scale bars: a and c, 1 μm b and d, 0.1 μm; e and g, 1 μm, f and h, 0.5 μm.

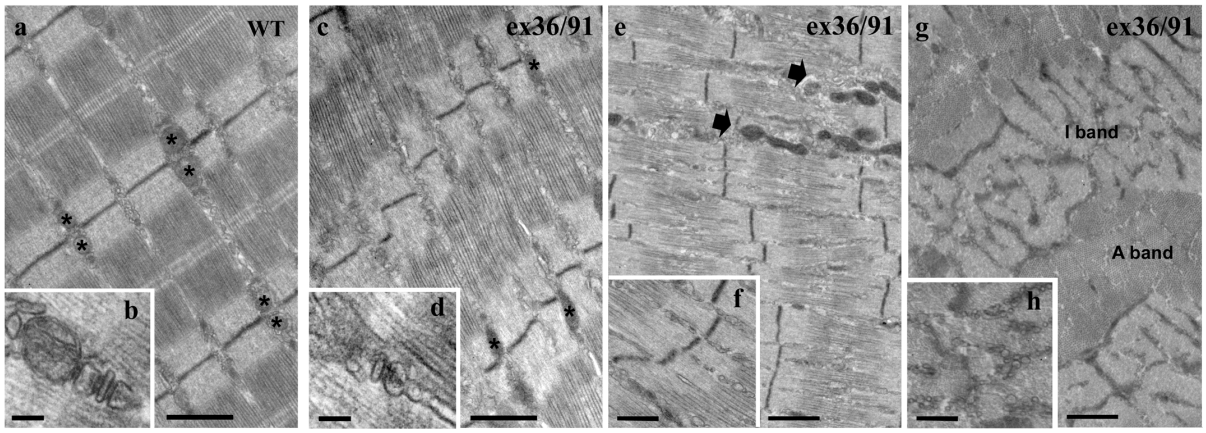

**Figure 8.** Electrically evoked peak $Ca^{2+}$ transients are reduced in muscle fibers from RyR1Q1970fsX16+A4329D mice. Enzymatically dissociated FDB**,** EDL and soleus fibers were loaded with Mag-Fluo-4 and electrically stimulated by field stimulation. Left panels show representative $Ca^{2+}$ transient elicited by a single 50 V pulse of 1 msec duration. Right panels show representative $Ca^{2+}$ transient elicited by a train of pulses delivered at 100 Hz for 300 msec. Black trace, WT; red trace, RyR1Q1970fsX16+A4329D.

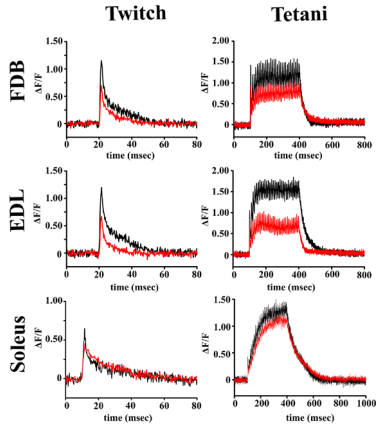

**Figure 9.** Gating characteristics of single RyR1 channels from skeletal muscle of RyR1Q1970fsX16+A4329D mice. **(a)** Representative mouse skeletal RyR1 single-channel current fluctuations from WT (left) and RyR1Q1970fsX16+A4329D mice (right) in the presence of 15 μM cytosolic $Ca^{2+}$ (top traces), 100 μM cytosolic $Ca^{2+}$ (middle traces) and 1 mM cytosolic $Ca^{2+}$ (bottom traces). The Po above each trace is the value determined over 3 min. O and C indicate the open and closed channel levels, respectively. **(b)** Single-channel current–voltage relationships for RyR1 channels from WT (squares) and RyR1Q1970fsX16+A4329D mice (triangles). **(c)** Relationship between cytosolic [$Ca^{2+}$] and RyR1 Po for channels derived from WT (squares) and RyR1Q1970fsX16+A4329D (triangles) mice. Error bars are s.e.m. for n= 12 (WT) and n=12-13 (RyR1Q1970fsX16+A4329D); $^{****}p < 0.0001$). Where not shown, error bars are within the symbol. **(d)** Mean Po values for single channels derived from either WT (white) and RyR1Q1970fsX16+A4329D (black) as indicated, in the presence of 15 μM $Ca^{2+}$ and 1 mM caffeine. Error bars are SEM for n = 12; $^{***}p < 0.001$.

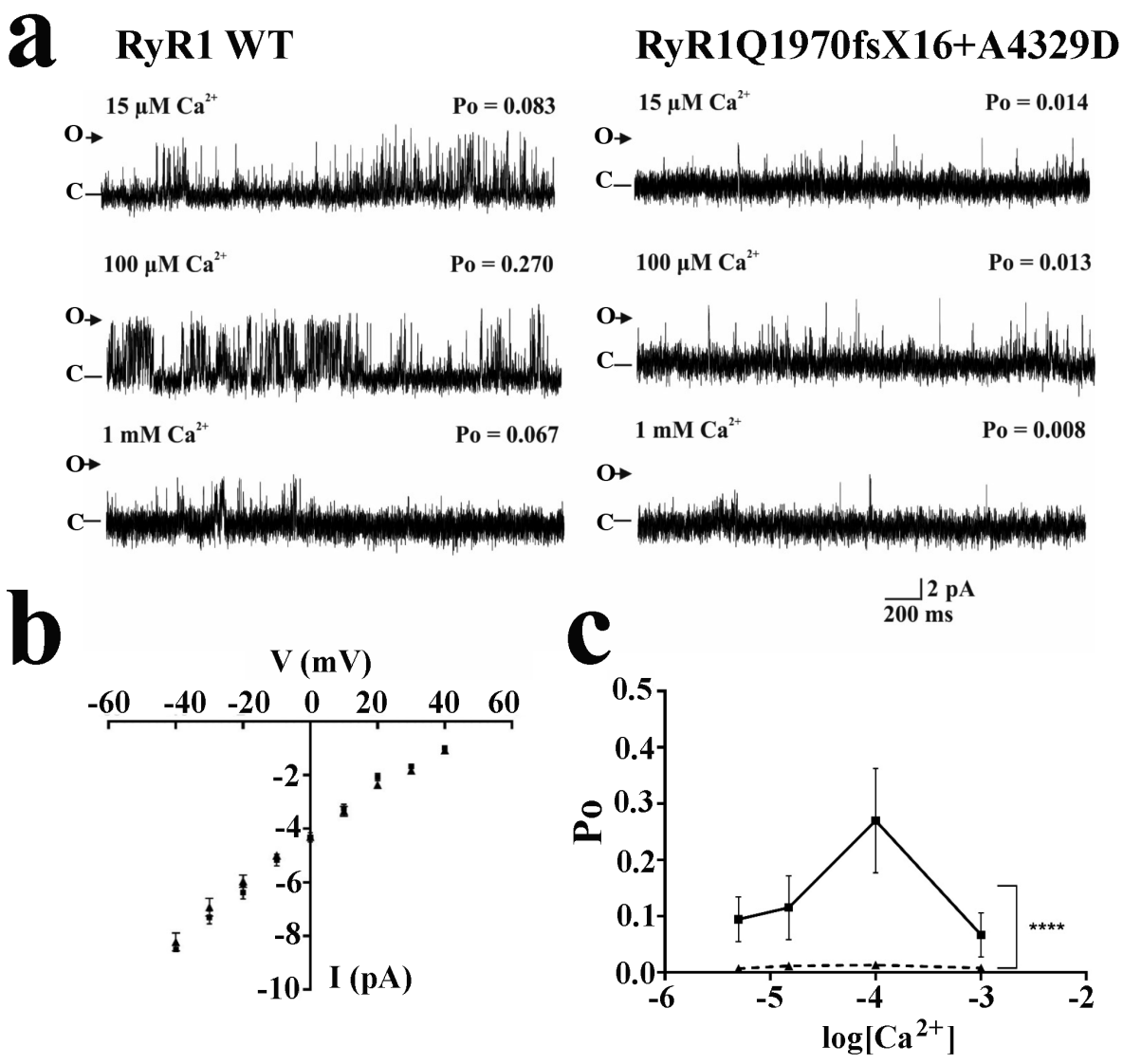

**Supplementary Table 1:** Sequence of primers used and target gene

**Supplementary Table 2:** List of antibody and suppliers

**Supplementary Table 3:** Twitch Kinetics and general parameters of EDL and soleus muscles from WT and RyR1Q1970fsX16+p.A4329D mice (values are the mean±S.D,)

**Supplementary Table 4:** Quantitative analysis of Calcium Release Units in EDL muscles from WT and RyR1Q1970fsX16+p.A4329D mice.

**Supplementary Table 5:** Analysis of electrically evoked calcium transients in FDB, EDL and soleus muscles from RyR1Q1970fsX16+p.A4329D and WT littermates.

**Supplementary Figure 1**: **Representative data of the ex36 RyR1 p.Q1970fsX16 and ex91 p.RyR1A4329D mutant mice**. Using CRISPR/Cas9 gene edition we generated mutations in exon 36 (**panel A**) and exon 91 (**panel B**) of the mouse RYR1 gene. Top panels show agarose gels of genomic DNA from the screening of the $F_0$ pups. Potential $F_0$ founders were identified by *PvuII* digestion of PCR fragments (arrows). Bottom panels show comparison of the cloned nucleotide sequence of WT and mutant mice; the small black arrows indicate insertion of the desired mutation. **(C)** and **(D)** show PAG electrophoresis of PCR products used for mouse genotyping of the $F_1$ offspring after digestion with *PvuII*.

**Supplementary Figure 2: Immunoreactivity of the antibodies used in the present study.** Total muscle homogenates were prepared from WT mice; proteins were separated on 7.5 % SDS PAG (left blots) or 10% SDS PAG (right blots) and probed with the indicated primary antibodies. Blots were then incubated with peroxidase conjugated anti mouse IgG or peroxidase conjugated protein-G and the bands were visualized by chemiluminescence.

**Supplementary Figure 3: Comparison of the growth curves of WT, *RYR1* heterozygous and compound heterozygous double mutant mice:** Body weight growth curves of male **(A)** and female **(B)** mice monitored for a period of 14 weeks. Each symbol shows the average (±S.D.) weight of n=11-13 mice. $p<0.05$ Mann-Whitney two tailed test for the compound heterozygous RyR1Q1970fsX16+p.A4329D (Ex36/Ex91) mice. Genotype symbols are shown on the bottom of the figure.

**Supplementary Figure 4: The RyR1 protein content in EDL muscles from WT and heterozygous ex91 is similar.** Total homogenates from EDL muscles from 3 WT and 3 RyR1 p.A4329D heterozygous mutant mice were pooled. Proteins were separated on a 6.5% SDS PAG, blotted overnight onto nitrocellulose and probed with anti-RyR1 Ab followed by anti-MyHC Ab for normalization.

# Abbreviations

CRU, calcium release units

DHPR, dihydropyridine receptor

ECC, excitation contraction coupling

EDL, *extensor digitorum longus*

FDB, *flexor digitorum brevis*

MmD, multiminicore disease

MyHC, myosin heavy chain

RyR1, ryanodine receptor 1

SERCA, sarco(endo)plasmic CaATPAse

SR, sarcoplasmic reticulum

TT, transverse tubules

WT, wild type